

M.L.G. JOY, V.P. LEBEDEV, R. MOON

Institute of Biomaterials and Biomedical Engineering, University of Toronto, Toronto, Ontario, Canada. M5S 3G9
+ Pavlov Institute of Physiology, Russian Academy of Sciences,

Current Density Imaging (1,2)

Introduction

- Current flowing in an object (Current Density, **J**) produces a magnetic field, **B**.
- The current Density, **J**, is related to **B** by the "CURL" ($\nabla \times$) operator:

$$\mathbf{J} = \nabla \times \mathbf{B}$$
- The vector components of the magnetic field **B** can be measured using a Magnetic Resonance Imager (MRI).
- Example $J_z = (B_y/x - B_x/y)$
- In a current density image (CDI) the brightness of each pixel is proportional to **J**, the component of **J** perpendicular to the image plane.

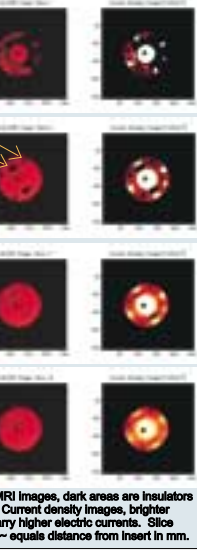


Example of Steps in making a CDI:

- Images were made of this cylinder (diameter 15cm, length 30 cm) containing salt water. Copper disk electrodes capped each end.
- A plastic rod ran diagonally between these electrodes.
- A smaller cylinder extended half way from one electrode to the other.
- Other inserts to constrain the current in the water could be added.
- The cylinder was placed in the bore of an MR Imager with its axis perpendicular to the main magnetic field (**B₀**).
- Bipolar AC pulses of Electric current were applied (200mA, 88ms).
- An MR image was taken of an axial slice.
- The cylinder was rotated about its axis and a second image was made.
- The 90 degree rotation was removed in the images to place the data in a coordinate system fixed in the cylinder.
- From the MRI data associated with these magnitude images, two MR phase images were constructed.
- The phase of these images is proportional to the component of **B** in the direction parallel to the main MRI magnetic field, **B₀**. Note the "wrapping" of the phase at radians.
- The phase was unwrapped and differentiated to form B_y/x and B_x/y images.
- These two images were then added and scaled to form a current density image.
- The colour of each pixel corresponds to the current density flowing out of the image. The units are Ampere per metre squared.
- Applied Current 200mA.
- Current measured from the image 191mA.
- Slice 5mm thickness. Pixel size 0.9mm

Example of CD images of constrained current flow.

- A plastic insert (sketched below) was placed in the cylinder used in the example above.
- The black areas correspond to a key, 4 rods and two 1cm high pegs holding the insert together. Both these (black) objects and the (white) plastic slab produce no MR signal and appear dark in the MRI images. The salt water appears bright.
- The Current Density images are of 1mm thick slices 5mm apart. Pixels are 0.9 mm square as before.
- Slice 1 was just at the upper boundary of the insert and at a small angle to it. The current is confined to flow through the large central hole and the five smaller holes around the edge.
- In slices 6, 11 and 16 the current slowly spreads to fill the large cylinder again.
- The applied current was 200mA and the currents measured from images 1, 6, 11 & 16 were 160, 186, 193 and 193mA respectively.



LEFT: MRI images, dark areas are insulators RIGHT: Current density images, brighter areas carry higher electric currents. Slice number = equals distance from insert in mm.

Transcranial Electrical Stimulation(3)

Introduction

It has been demonstrated in experiments and in clinical practice (4) that TCES with specific parameters elicits profound analgesia without side effects. This type of TCES is effective only if current is applied in the sagittal section. This non-pharmacological intervention is presently used in hospitals and outpatient clinics for treating pain syndromes and during surgical anaesthesia to replace morphine-like analgesics. Data have been obtained which clearly indicate that this type of analgesia has a pure endorphinergic nature (5). Thus there is the possibility, that this type of TCES could activate the endorphinergic and related antinociceptive structures located in deep brain stem structures - in the hypothalamus, midbrain, and medulla (6). We wished to determine the magnitude of the current density in these structures without damaging the brain and skull.

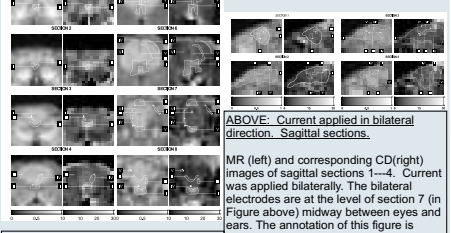
Method

Imaging experiments were done on 4 New Zealand rabbits (2.6-3.5kg body weight), anesthetized (Nembutal, 35mg/kg i.p.), paralysed (Pavulon, 0.5mg/kg, i.v.) and artificially. During the experiment, additional dosages of these drugs were injected periodically if necessary. Five copper electrodes (1cm each) were inserted under the skin through small incisions and fixed by sutures. The electrodes were positioned one on the forehead and two symmetrically on the both sides of the head between the eyes and ears, and one behind each ear. For the sagittal direction of current the electrode on the forehead and the pair behind ears were used. The other pair of electrodes was used for bilateral oriented current application. The heads were firmly fixed in a plastic stereotaxic frame with an angle of about 51 between the zygomatic tooth bar line and the base of the frame (see Shek (14)). The stereotaxic frame was designed to maintain the rabbits in both the horizontal (prone) and vertical position. These positions made the MRI "coronal" slices and "sagittal" slices correspond closely to those in three-dimensional atlas maps (14) allowing easier identification of the levels and structures.

LF CDI images (3mm slices, no gap between slices, 0.78mm pixels) were made with both a coronal (8 slices) and a sagittal (4 slices) orientation. Bipolar (19mA 40ms duration) current was applied in the sagittal and bilateral directions (respectively) so that the current was approximately orthogonal to the slice in each case.

Results

The figures below show details of the current density that arose from sagittal and bilateral application of current. The CD images show regions of high and low current which seem to be related to the anatomy of the brain. The high CD regions coincided with cerebrospinal fluid (CSF) surrounding the brain.



ABOVE: Current applied in Sagittal direction. Coronal sections

MR (left) and corresponding CD (right) images of sagittal sections 1-4. Current was applied bilaterally. The bilateral electrodes are at the level of section 7 (in Figure above) midway between eyes and ears. The annotation of this figure is different than that used in the Figure on the left. The contours which were based on the MRI image (left) are drawn only on that image and not on the corresponding CD image (right), and vice versa. The Roman numerals associated with all the contours and the line which joins them to their contour is shown on both MRI and CD images. The Roman numerals with an asterisk are associated with contours drawn on the CD images to surround regions of high current. Numbers in brackets are average CDs, in A/m, at the pixel or in the contour indicated.

- Section 1: I-Olfactory bulb(5.8); II-Space between bulbs (19.7)
 Section 2: I-Longitudinal fissure(19.1); II-Rhinal fissure(16.8).
 Section 3: I-Longitudinal fissure(5.8); II-Ventrolateral surface, Basal cisterna(17.6); III-Lateral ventricle(10.0).
 Section 4: I-Chiasmatic(15.8); II-Chiasmatic cisterna(15.1); III-Cerebrum semiovalis(2.6); IV-Lateral ventricle(7.9).
 Section 5: I-Basal cisterna(12.2); II-Longitudinal fissure(9.1); III-Region of dorsal part of Third ventricle(7.3); IV-Ventral recess of Third ventricle (7.4); V-Space below pallidum(6.5); VI-Thalamus(4.2).
 Section 6: I-Cisterna interpeduncularis(9.4); II-Dorso-lateral cortex(6.9); III-Space around brain stem(5.5); IV-Longitudinal fissure(15.6); V-Third ventricle(10.6); VI-Thalamus(2.3).
 Section 7: I-Dorso-lateral cortex(9.1) II-Region above colliculi(10.1); III-Interpeduncularis(7.3); IV-Rostal part of lateral ventricle(5.7); V-Fissure between hemispheres and cerebellum(11.0). The CD scale is the same as in the on the left.

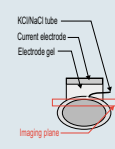
LEFT Below: Some horizontal reconstructions of CP's of sagittally applied current through horizontal sections of the rabbit brain digitally created from coronal CD images (see above left).
 Section 6: SpM-CP in space above midbrain. d. AqV-CP in the third ventricle and aqueductus. Section 7: LV-CP in rostral parts of lateral ventricles. Section 8: CP's in basal cisterna. SF-space between frontal lobes; Ch-chiasmatic cisterna; PG-position of brain stem(10.8 10.0); IV-aqueductus(5.7); V-Lateral ventricle(7.4).
 Section 4: I-Contour of the skull core(6.9); II-Lateral ventricle(5.8); III-Fissure between hemispheres and cerebellum(11.0). The CD scale is the same as in the on the left.

Spreading Depression

Introduction

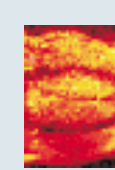
SD can be elicited by electrical, mechanical or chemical stimuli (7) to the cortex (with dura mater removed). A small direct current pulse, a needle prick and a high concentration of KCl are respective examples of these stimuli. SD is characterized by a slowly moving wave of loss of spontaneous and evoked neural activity, a sudden and pronounced negative shift in the extracellular potential and a complete or near-complete depolarization of neurons and glia. A massive redistribution of ions between the extracellular and intracellular spaces and changes in regional cerebral blood flow (rCBF) are also observed during SD (8).

As its name suggests, SD spreads from the site of initiation as a concentric wave moving at 2.7.5 mm/min (somewhat faster in hippocampus than in neocortex). This depression of electrical activity is self-propagating and can only be prevented by a physical block or by using specific chemicals such as Ca²⁺ channel blockers. The depression of electrical activity is preceded by a synchronous depolarization of all neuronal tissues encountered by the wave front. This depolarization is immediately followed by a repolarization and an extended period of hyperpolarization. The SD mechanism is not based on an action potential (which would propagate at a much higher speed (9)). The traveling wave of SD usually stops at the border of white matter. However, it affects the tissue characteristics of surrounding underlying white matter (10). Since SD does not propagate through the white matter of the contra lateral cortex (in the case of cortical SD) is unaffected by SD. Gray matter affected by SD recovers to a pre-SD state after 40 to 60 min of rest. After a sufficient resting period, another SD can be elicited with similar stimuli (11).



Methods

Male Wistar rats (350g to 400g) were anesthetized with an intra-peritoneal injection of sodium pentobarbital (50mg/kg) and was secured to a stereotaxic frame. A subsequent top-up dose (0.1cc i.m.) was administered to maintain the surgical anaesthesia. The skin and the muscle on top of the skull were removed to ensure good electrical contact between the electrode and the skull. Current was injected from the top of the cortex into the brain through an electrode to the top of the skull with a return electrode on the roof of the animal's mouth. To avoid artifacts the metal part (chlorided silver plate (0.5 mm thick) of the skull electrode was separated from the skull by a chamber filled with highly conductivity electrode gel (Figure on left). Two burr holes (1 & 4mm lateral from the bregma) were made over one hemisphere of the cortex for the delivering of KCl and for the recording electrode. The dura mater was removed in the lateral opening and KCl (20% w/w) was delivered to the cortical surface using a 10 gauge polyethylene tubing positioned over the opening. A Hamilton syringe allowed for an accurate release of KCl in steps of 0.05µl. An insulated fine copper wire (0.3mm) was inserted into the medial opening to record DC potential. An RF CDI image (2mm thick slice, 0.31mm pixels) was made with the slice orientation shown in Figure 3. The RF current pulse was 20ms duration. The imaging was timed so that the whole of the imaged affected cortical hemisphere would be depressed during the 394s required to obtain them.



Results

A typical current density map is shown in Figure on left. Although the current was passed through the intact skull, the CD maps showed a good current penetration over the two hemispheres of the cortex (average CD of 173 A/m²). The CD inside the skull remained stable, fluctuating less than 9% of the mean current density over 5 RF-CD sessions. Some current flow was also observed outside the skull in the surrounding muscle/skin area and in the eyes. The electrode configuration provided uniform current density over the cortex without causing any artifacts due to the susceptibility mismatch. Unlike the cortex, the CD outside of the skull was not uniform showing patches of high intensity areas. One exception was a consistent high current density observed over both eyes of the animal (413 A/m²). Although the CD image is noisy, a clear definition of both hemispheres of the cortex and the surrounding structures such as the skull, eyes, and the outer muscle/skin are visible. During SD the current density in the affected hemisphere increases by 20 to 100% while that on the contra lateral side changes by 15 (decrease) to +38% (increase).

Conclusion

Current density imaging has the potential to be of use to those studying functional electrical stimulation. It will allow them to measure the current distributions produced by stimulating electrodes. LFCDI is the most accurate CDI method. All that is required is access to an MR imager and some basic knowledge of the physics

References

1. M. L. G. Joy, G. Scott, R. M. Henkelman, *Magn. Reson. Imaging* 7, 89-94 (1989).
2. K. Beravs, M. L. G. Joy, R. Frangez, F. Demsar, (1998); I. Sersa, K. Beravs, N. F. J. Dodd, S. Zhao, F. Demsar, *In Vivo MRI Determination of Electric Current Density in Mice Tumours - a New Approach for Monitoring the Efficiency of Electrochemo Tumour Therapy*, Proceedings of the Soc. Mag. Res. and Europ. Soc. For Mag. Res. in Med. and Biol., Nice (1995); B. M. Eyboglu, R. Reddy, J. S. L. Jr., *Imaging of Electric Current Density with MRI Imaging*, Proceedings of the RSNA (RSNA Proceedings, 1996); H. R. Gamba, D. T. Delopy, *Medical and Biological Engineering and Computing* 36, 165-170 (1998); G. C. Scott, M. L. G. Joy, R. L. Armstrong, R. M. Henkelman, *IEEE Trans. Med. Imaging* 10, 362-374 (1991); G. C. Scott, M. L. G. Joy, R. L. Armstrong, R. M. Henkelman, *IEEE Transactions on Medical Imaging* 14, 515-524 (1995); G. C. Scott, M. L. G. Joy, R. L. Armstrong, R. M. Henkelman, *Magnetic Resonance in Medicine* 33, 355-369 (1995); G. C. Scott, M. L. G. Joy, R. L. Armstrong, R. M. Henkelman, *J. Magn. Reson.* 97, 235-254 (1992); G. C. Scott, M. L. G. Joy, R. L. Armstrong, R. M. Henkelman, *Magn. Reson. Med.* 28, 186-201 (1992).
3. M. L. G. Joy, V. P. Lebedev, J. Gatti, *IEEE Transactions on Biomedical Engineering* 46, 1139-1149 (1999).
4. V. P. Lebedev, J. S. Katznelson, V. A. Leosko, A. Baranovski, G. I. Shlemis, *Fiziol. Zhurn. SSSR im. Sechenova* 68, 1120 - 1123 (1983); V. P. Lebedev, *New Method of Transcranial Electroanalgesia*, V.P. Lebedev, Ed. (Nauka, Leningrad, 1987); S. I. Gretzov, A. Zhurn, *nevroptatologii i psikhiatrii im. Korsakova XXXX*, 1800 - 1804 (1987); V. P. Lebedev, *In Pain Syndrome Y.D. Ignatov, V. A. Mokhalovits, Eds. (Medicina, 1990)*, pp. 162-172.
5. L. N. Airapetov et al., *Fiziol. Zhurn. SSSR im. Sechenova* 71, 56 - 63 (1985); V. P. Lebedev, A. B. Savchenko, N. V. Petyaevskaya, *Fiziol. Zhurn. SSSR im. Sechenova* 74, 1246 - 1256 (1988).